

Surface melting of the vortex lattice

A. De Col¹, G.I. Menon², V.B. Geshkenbein^{1,3}, and G. Blatter¹

¹*Theoretische Physik, ETH-Hönggerberg, CH-8093 Zürich, Switzerland*

²*The Institute of Mathematical Sciences, C.I.T. Campus, Taramani, Chennai 600 113, India and*

³*L.D. Landau Institute for Theoretical Physics, RAS, 117940 Moscow, Russia*

(Dated: November 21, 2018)

We discuss the effect of an (*ab*)-surface on the melting transition of the pancake-vortex lattice in a layered superconductor within a density functional theory approach. Both discontinuous and continuous surface melting are predicted for this system, although the latter scenario occupies the major part of the low-field phase diagram. The formation of a quasi-liquid layer below the bulk melting temperature inhibits the appearance of a superheated solid phase, yielding an asymmetric hysteretic behavior which has been seen in experiments.

PACS numbers: 74.25.Qt, 74.25.Dw, 68.35.Rh

The transition between vortex solid and vortex liquid phases observed in the mixed phase of high- T_c superconductors [1] has generated renewed interest in the problem of melting. In common with other discontinuous phase transitions, melting should involve the appearance of both metastable undercooled liquid and overheated solid phases. Hence, hysteretic behavior is expected upon cycling through the transition. However, experiments on the layered, high- T_c superconductor BiSSCO [2] reveal an asymmetric hysteresis, characterized by the appearance of only the supercooled liquid and no overheated solid. Similar behavior is displayed by ordinary crystals [3, 4], where such asymmetry is understood to be a consequence of surface (pre-)melting: surfaces act as nucleation centers for the liquid, thereby inhibiting the metastable solid above the melting transition. However, such surface melting is not generic and there are experimental systems where the surface remains solid up to the bulk melting transition [4]. In this letter, we study the effects of an (*ab*)-surface on vortex lattice melting, showing that as the strength of the magnetic field is varied, the *same* surface may exhibit *either* ‘surface non-melting’ or ‘surface melting’ behavior. The latter scenario applies to the major part of the low-field phase diagram, in agreement with experiments [2].

Early studies [5] of simple crystals have focused on the solid phase and have demonstrated that the surface turns unstable before the bulk melts. Going beyond such a stability analysis is a difficult task, as a theory is required which describes both solid and liquid phases in a unified manner. Qualitative insight can be gained from a Landau theory [6] by including the destabilizing effect of the surface: two melting scenarios are found, surface melting (O_2) with a continuous- and surface non-melting (O_1) with a discontinuous vanishing of the order parameter at the surface. More elaborate *ab initio* calculations reduce the problem to a mean-field order-parameter theory and determine the free energy either as a lattice sum [7] or within a density functional theory (DFT) [8] exploiting liquid-state correlations.

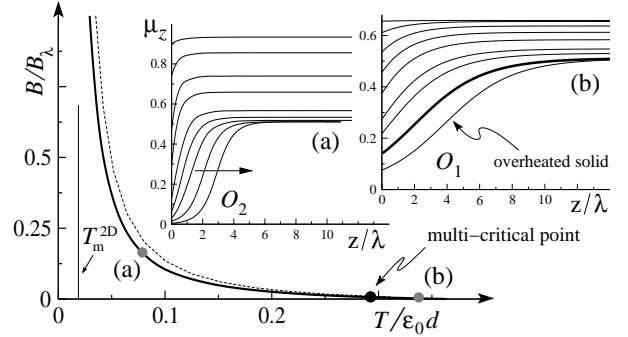


FIG. 1: Comparison of the melting line $B_m(T)$ obtained via the DFT-substrate approach (present work, full line) with that of Ref. [10] (dashed line). Top right: Numerical solutions of the order-parameter profile μ_z for different fields B increasing from top to bottom: (a) at $T = 0.08 \epsilon_0 d$ (O_2 transition with the liquid-solid interface invading the bulk as $B \nearrow B_m$) and (b) at $T = 0.33 \epsilon_0 d$ (O_1 transition with the thick line corresponding to $B = B_m$).

The vortex matter in Bi- and Tl-based high- T_c superconductors is characterized by an extreme anisotropy: pancake-vortices confined to superconducting layers exhibit repulsive logarithmic interactions within the planes and weakly attractive inter-layer interactions extending over many layers (see, e.g. Ref. [9]; we ignore here a weak Josephson coupling between the layers). These anisotropic properties inspire the use of a substrate-mean-field theory [10] describing the vortex system in terms of two-dimensional lattices of pancake-vortices subject to a substrate potential generated by the mean action of the vortices residing in other layers. The bulk melting line is known [9, 10, 11, 12] to interpolate between the Berezinskii-Kosterlitz-Thouless (BKT) transition temperature $T_{\text{BKT}} \lesssim T_c$ of the individual layers at zero external field and the two-dimensional vortex-lattice melting temperature $T_m^{2D} \ll T_c$ at high magnetic fields, see Fig. 1. We use the classical DFT of freezing [13] and exploit the anisotropic properties of the system with its natural separation of liquid-state correlations into in-

plane and out-of-plane components. As a result, we obtain a reliable and analytically tractable order-parameter theory which allows us to study (*ab*)-surface melting. We find two regimes within the B - T phase diagram: for low and high magnetic fields B the surface order parameter undergoes a finite, although reduced, jump (O_1) at the bulk melting temperature, whereas for intermediate values of B , stray magnetic fields destabilize the layers close to the surface, leading to the surface melting scenario (O_2).

We sketch the derivation of pancake-vortex interactions in a semi-infinite superconductor filling the half-space $z \geq 0$. These interactions are mediated by currents set up by the vortices via the Lorentz force (here, d is the layer separation, λ the London penetration depth, and Φ_0 the flux unit): each vortex generates a current density $\mathbf{j} = -(c/4\pi\lambda^2)[(\Phi_0/2\pi)\nabla\varphi + \mathbf{A}]$ which acts on another vortex core with a transverse force $\mathbf{F} = d\Phi_0 \mathbf{z} \times \mathbf{j}/c$. For a co-planar pair of pancake-vortices the current density is driven by the phase gradient $\nabla\varphi = -\mathbf{n}_z \times \mathbf{R}/R^2$ and the force $\propto 1/R$ produces a long-range logarithmic repulsion $V_{z,z}(R) \approx -2\varepsilon_0 d \ln(R/\xi)$; this potential corresponds to that of a one-component charged plasma (OCP) with charge $e^2 \rightarrow 2\varepsilon_0 d$ and $\varepsilon_0 = (\Phi_0/4\pi\lambda)^2$ the vortex line energy. The interaction between two pancake-vortices residing in different layers derives from the vector potential \mathbf{A} ; calculating the field associated with a pancake-vortex in a semi-infinite geometry and integrating the Lorentz force provides the potential

$$V_{z,z'}(R) = -\varepsilon_0 d^2 \int_0^\infty dK \frac{J_0(KR)}{\lambda^2 K K_+} \times [f_{z-z'}(K) + \beta(K)f_{z+z'}(K)] \quad (1)$$

with $f_z(K) = \exp(-K_+|z|)$, $K_+ = \sqrt{K^2 + \lambda^{-2}}$, and $\beta(K) = (K_+ - K)/(K_+ + K)$. The bulk term $\propto f_{z-z'}$ is augmented by a stray-field term $\propto f_{z+z'}$ relevant within a distance λ from the surface. For small in-plane distances $R \ll \lambda$, the contribution of the stray-field term can be neglected and we recover the bulk expression $V_{z,z'}(R) \approx \varepsilon_0 d(dR/\lambda^2)[R/(R+4|z-z'|)]$ [9]. For a large separation $R \gg \lambda$, the surface term is relevant and we obtain

$$V_{z,z'}(R) \approx 2\varepsilon_0 d [\phi_t(z, z') \ln(R/\lambda) + (d/R)e^{-(z+z')/\lambda}],$$

where $\phi_t(z, z') = (d/2\lambda)(e^{-|z-z'|/\lambda} + e^{-(z+z')/\lambda}) \ll 1$ is the fraction of flux trapped in the layer z' generated by a pancake-vortex at z : a test vortex at z' then effectively experiences a logarithmic attraction from *two* bulk-type pancake-vortices, the real one at z and a fake mirror vortex with equal sign at $-z$, the latter generated by the stray field. The algebraic repulsion associated with the second term in $V_{z,z'}(R)$ is again due to the stray field and produces a surface softening.

In our investigation of the vortex solid-liquid transition we make use of the classical density functional theory

(DFT) [13] which builds on the (grand canonical) free-energy difference $\delta\Omega = \Omega_{\text{sol}} - \Omega_{\text{liq}}$ expressed through the variation $\delta\rho(\mathbf{r}) = \rho(\mathbf{r}) - \bar{\rho}$ in particle density away from the uniform liquid state density $\bar{\rho}$; for the inhomogeneous and anisotropic vortex matter system, $\delta\rho_z(\mathbf{R}) = \rho_z(\mathbf{R}) - \bar{\rho}$ and $\bar{\rho}$ is the 2D liquid density,

$$\frac{\delta\Omega[\rho_z(\mathbf{R})]}{T} = \int \frac{dz}{d} d^2\mathbf{R} \left[\rho_z(\mathbf{R}) \ln \frac{\rho_z(\mathbf{R})}{\bar{\rho}} - \delta\rho_z(\mathbf{R}) - \frac{1}{2} \int \frac{dz'}{d} d^2\mathbf{R}' \delta\rho_z(\mathbf{R}) c_{z,z'}(|\mathbf{R}-\mathbf{R}'|) \delta\rho_{z'}(\mathbf{R}') \right]. \quad (2)$$

The first two terms describe the entropic contribution of a non-interacting gas, while the last term accounts for the microscopic interactions $V_{z,z'}(R)$ via the direct pair-correlation function $c_{z,z'}(R)$ of the liquid state; in the homogeneous liquid, the (dimensionless) Fourier transform $c_{k_z}(K) = (\bar{\rho}/d) \int d^3r c_z(R) e^{-i\mathbf{k}\cdot\mathbf{r}}$ is related to the static structure factor via $S(\mathbf{k}) = 1/[1 - c_{k_z}(K)]$. The appearance of finite density-modulations $|\delta\rho_z(\mathbf{R})| > 0$ in the solid is a consequence of these correlations. We exploit the anisotropy of the pancake-vortex system and separate $c_{z,z'}(K)$ into in- and out-of-plane parts,

$$c_{z,z'}(K) = c^{2D}(K) d \delta(z-z') - V_{z,z'}(K)/T, \quad (3)$$

where $c^{2D}(K)$ denotes the correlation function of the 2D-OCP as obtained from standard Monte-Carlo simulations [14]. The second term accounts for the weak inter-plane interactions; within lowest-order perturbation theory [15] it is given by the Fourier transform of the out-of-plane interaction (1), $V_{z,z'}(K)/T = -\alpha(K)[f_{z-z'}(K) + \beta(K)f_{z+z'}(K)]$ with $\alpha(K) = 2\pi\varepsilon_0 d^2 \bar{\rho}/T \lambda^2 K^2 K_+$.

We begin with the homogeneous bulk system. Consider the Fourier transforms $\delta\rho_z(\mathbf{K}_n)/\bar{\rho}$ for the density field and $\xi_z(\mathbf{K}_n)$ for the molecular field [13] $\xi_z(\mathbf{R}) \equiv \ln[\rho_z(\mathbf{R})/\bar{\rho}]$, where \mathbf{K}_n denote the reciprocal triangular-lattice vectors. For a correlation function $c^{2D}(K)$ decaying rapidly beyond the first reciprocal lattice vector, only the first two components need be retained and we can restrict the Ansatz to the form $\delta\rho_z(\mathbf{R})/\bar{\rho} \approx \eta_z + \mu_z g(\mathbf{R})$ and $\xi_z(\mathbf{R}) \approx \kappa_z + \xi_z g(\mathbf{R})$ with $g(\mathbf{R}) = \sum_{|\mathbf{K}_n|=G} \exp(i\mathbf{K}_n \cdot \mathbf{R})$, $G = 4\pi/\sqrt{3}a_\Delta$ (a_Δ the lattice constant, $a_\Delta^2 = 2\Phi_0/\sqrt{3}B$). Furthermore, κ_z and ξ_z are related to μ_z via [16]

$$\kappa_z = -\Phi(\xi_z), \quad \mu_z = \Phi'(\xi_z)/6, \quad (4)$$

with $\Phi(\xi) = \ln s^{-1} \int_s d^2R \exp[\xi g(R)]$ and Φ' its derivative (here, s denotes the 2D unit cell area). Inserting this Ansatz into the free-energy density (2), we obtain the reduced functional for a bulk system in the form (we use the normalization $\delta\omega = \delta\Omega/T S \bar{\rho}$ with S the sample area)

$$\frac{\delta\omega[\mu_z]}{T} = \int \frac{dz}{d} \left[\frac{\delta\omega_{\text{sub}}^{2D}(\mu_z)}{T} + \frac{3\bar{\alpha}}{2} \int \frac{dz'}{d} \bar{f}_{z-z'}(\mu_z - \mu_{z'})^2 \right],$$

with $\bar{\alpha} = \alpha(G)$ and $\bar{f}_{z-z'} = f_{z-z'}(G)$. The first term describes the free-energy density of individual layers

$$\frac{\delta\omega_{\text{sub}}^{2D}(\mu_z)}{T} = \kappa_z(\mu_z) + 6\xi_z(\mu_z)\mu_z - 3 \left[\bar{c}^{2D} + \frac{2\bar{\alpha}}{dG_+} \right] \mu_z^2, \quad (5)$$

with in-plane correlations $\bar{c}^{2D} \equiv c^{2D}(G)$ and out-of-plane correlations described by the substrate potential $-\bar{\alpha} \int (dz/d) \bar{f}_z = -2\bar{\alpha}/d G_+$ with $G_+ = \sqrt{G^2 + \lambda^{-2}}$. Note that both κ_z and ξ_z have to be understood as functions of the order-parameter μ_z via (4). The second non-local term in $\delta\omega$ accounts for inhomogeneities of the order-parameter field μ_z and involves the dispersive ‘elastic coefficient’ $\bar{\alpha} \bar{f}_{z-z'}$. Here, we neglect the small change in density across the transition described by η_z ; its inclusion involves a more elaborate analysis accounting for the discrete nature of the particles [14].

The bulk melting line $B_m(T)$ is obtained from minimizing the functional $\delta\omega[\mu]$ for a homogeneous order parameter μ . At large values of B , the inter-planar interaction is negligible and the melting temperature is given by the solid-liquid transition of the 2D-OCP [13] as described by the free-energy density (5) without substrate potential (termed $\delta\omega^{2D}$). For small \bar{c}^{2D} (large temperatures), $\delta\omega^{2D}(\mu)$ exhibits only the liquid minimum at $\mu_{\text{liq}} = 0$, cf. Fig. 2. Lowering the temperature, the correlator \bar{c}^{2D} increases and $\delta\omega^{2D}(\mu)$ develops a second minimum at a finite value of μ describing the solid phase. At the critical value $\bar{c}^{2D} = \bar{c}_c = 0.856$ the ‘solid’ minimum drops below the ‘liquid’ one and the high-field liquid-solid transition takes place. The comparison with numerical simulations [17] allows us to check the accuracy of our approach: Monte Carlo simulations [17] show that the 2D-OCP freezes at $T_m^{2D} \approx \varepsilon_0 d/70$ where the correlator assumes the value $\bar{c}^{2D} \approx 0.77 < \bar{c}_c$; more sophisticated versions of DFT cure this discrepancy [18].

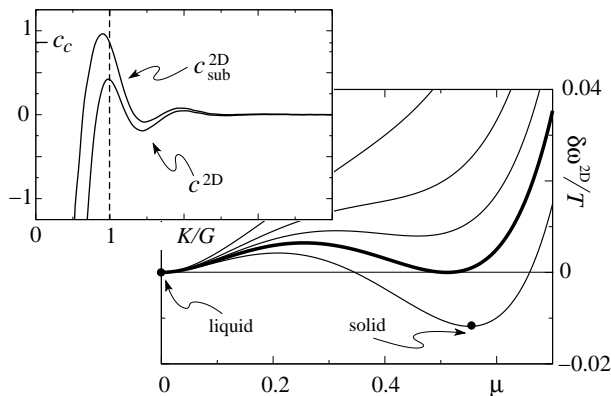


FIG. 2: Top left: direct pair-correlation functions at $T/\varepsilon_0 d = 0.08$ for the 2D-OCP, $c^{2D}(K)$ from MC simulations and $c_{\text{sub}}^{2D}(K) = c^{2D}(K) + 2\alpha(K)/dK_+$ for the full 3D system at melting ($B = B_m$). Bottom right: Free energy $\delta\omega^{2D}(\mu)/T$ for values $\bar{c}^{2D} = 0.80, 0.83, 0.845, 0.856 (= \bar{c}_c \text{ critical value, thick line}), 0.87$. At melting the order parameter jumps from $\mu_{\text{sol}} \approx 0.51$ to $\mu_{\text{liq}} = 0$.

At low B ($< B_\lambda \equiv \Phi_0/\lambda^2$), the inter-planar correlations become relevant and the 2D correlations \bar{c}^{2D} are augmented by the substrate potential. The condition $\bar{c}_c = \bar{c}^{2D} + 2\bar{\alpha}/dG_+ = \bar{c}^{2D} + (\sqrt{3}\varepsilon_0 d/2\pi T)[1 +$

$(8\pi^2/\sqrt{3})B/B_\lambda]^{-1}$ yields the bulk melting line

$$\frac{B_m(T)}{B_\lambda} = \frac{\sqrt{3}}{8\pi^2} \left[\frac{\sqrt{3}\varepsilon_0 d}{2\pi T[\bar{c}_c - \bar{c}^{2D}(T)]} - 1 \right]. \quad (6)$$

Given the temperature dependence of the OCP correlator $\bar{c}^{2D}(T)$ as an input, we obtain the full melting line as shown in Fig. 1; our result agrees well with those from numerical simulations [12] and improves upon results obtained from other liquid-state closure schemes [11].

Surface melting involves a non-uniform order-parameter field μ_z defined in a half-infinite sample $z > 0$. The translation-invariant correlator $\propto \bar{f}_{z-z'}$ in $\delta\omega$ now has to be replaced by the full expression $V_{z,z'}(G)/T$ with additional mirror and surface terms. Minimization with respect to μ_z provides us with the integral equation

$$\frac{\partial_{\mu_z} \delta\omega_{\text{sub}}^{2D}(\mu_z)}{T} + 6\bar{\alpha} \int_0^\infty \frac{dz'}{d} [\bar{f}_{z-z'} + \bar{f}_{z+z'}](\mu_z - \mu_{z'}) + \frac{12\bar{\alpha}G}{G+G_+} \int_0^\infty \frac{dz'}{d} \bar{f}_{z+z'} \mu_{z'} = 0. \quad (7)$$

The order parameter profile μ_z can be calculated numerically and we show two typical examples in Fig. 1: while we find the surface order-parameter μ_0 to vanish smoothly at $T = 0.08 \varepsilon_0 d$ (O_2 scenario), a residual jump in μ_0 is obtained at the higher temperature $T = 0.33 \varepsilon_0 d$ (O_1). In the following, we locate the multi-critical point T_{mc} on the melting line $B_m(T)$ separating the continuous O_2 - from the discontinuous O_1 regime.

To make progress analytically, we have to simplify the non-local terms in (7). Concentrating on the bulk, a gradient expansion of the term $\propto \bar{f}_{z-z'}$ leads us to the differential equation (we define $\partial_z \mu_z \equiv \mu_z'$)

$$\ell^2 \mu_z'' = \partial_{\mu_z} \delta\omega_{\text{sub}}^{2D}(\mu_z)/T \quad (8)$$

with $\ell^2 = (6\bar{\alpha}/d) \int dz \bar{f}_z z^2 = 12\bar{\alpha}/dG_+^3$. This local approximation is valid if the profile μ_z varies slowly over the extension G_+^{-1} of the kernel; we have verified that this condition is fulfilled for $T \gtrsim 0.04 \varepsilon_0 d$ (corresponding to $B \lesssim 0.5 B_\lambda$). Equation (8) has to be completed with a boundary condition. Close to T_{mc} , the order parameter μ_z is small near the surface; linearizing $\partial_{\mu_z} \delta\omega_{\text{sub}}^{2D}/T \approx 6(1 - \bar{c}_c)\mu_z$ in (7) we obtain the equation

$$\mu_z = \frac{G_+}{2(1+r)} \int_0^\infty dz' [\bar{f}_{z-z'} + \bar{\beta} \bar{f}_{z+z'}] \mu_{z'} \quad (9)$$

with $r = dG_+(1 - \bar{c}_c)/2\bar{\alpha}$ and $\bar{\beta} = (G_+ - G)/(G_+ + G)$. While the solution of this type of integral equation is a non-trivial task in general, a straightforward solution is possible in the present case due to the particular exponential structure of the kernel. Taking the second derivative of (9), we obtain the differential equation $\ell^2 \mu_z'' = 6(1 - \bar{c}_c)\mu_z$, which shows no trace of the boundary term $\propto \beta$ and thus coincides with the bulk equation

(8) at small μ_z [19]. This equation then admits the exponential solution $A \exp(\sqrt{r}G_+z) + B \exp(-\sqrt{r}G_+z)$ and inserting this Ansatz back into (9) the boundary term fixes the ratio A/B ; as a result, we obtain the boundary condition

$$[\mu'_z/\mu_z]_{z=0} = G_+(1-\beta)/(1+\beta) = G. \quad (10)$$

The analysis of the boundary value problem (8) with (10) follows the one in Ref. [6]: Combining the boundary condition (10) with the expression for the ‘conserved energy’ $(\ell \mu'_z)^2 - 2\delta\omega_{\text{sub}}^{2\text{D}}(\mu_z)/T = 0$, we find the relation

$$\mu_0 \ell G = \sqrt{2\delta\omega_{\text{sub}}^{2\text{D}}(\mu_0)/T}. \quad (11)$$

The liquid surface $\mu_0 = 0$ is always a solution and we deal with a continuous surface melting (O_2 scenario) if it is the only one. Once a second solution with $\mu_0 > 0$ is present, the surface undergoes a discontinuous O_1 transition. The O_1 - and O_2 scenarios are separated by a multi-critical point: expanding $\delta\omega_{\text{sub}}^{2\text{D}}$, we find that (11) admits two solutions for $T > T_{\text{mc}} \approx 0.29 \varepsilon_0 d$ ($B_{\text{mc}} \approx 0.007 B_\lambda$) and the surface (non)-melting is realized for $T < T_{\text{mc}}$ ($T > T_{\text{mc}}$). In Fig. 3, we show the solution of (11) and compare it with numerical results.

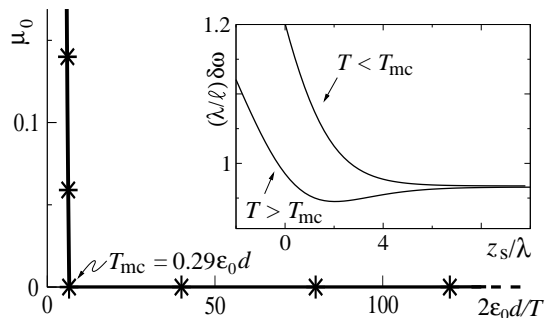


FIG. 3: Order parameter μ_0 at the surface: analytic (see Eq. (11), solid line) and full numerical solution (stars). Inset: energy as a function of soliton position z_s . Note the minimum for $T = 0.33 \varepsilon_0 d > T_{\text{mc}}$ (O_1 , pinned soliton) which has disappeared at $T = 0.28 \varepsilon_0 d < T_{\text{mc}}$ (O_2 , depinned soliton).

The appearance of the multi-critical point ($T_{\text{mc}}, B_{\text{mc}}$) can be interpreted as a surface-depinning transition of the solid-liquid interface (soliton): the energy cost to push this soliton into the system generates a repulsive potential, while the surface term favoring the liquid phase helps the soliton to enter, see Fig. 3. With decreasing temperature the stable minimum close to the surface (generating a finite μ_0 and leading to a O_1 transition) moves deeper into the bulk and disappears altogether at T_{mc} . As a consequence, the (half-height) position z_s of the solitonic solid-liquid interface diverges logarithmically into the bulk [6] as $T \rightarrow T_m$ from below, $z_s \sim |\ln(T_m - T)|$, within the entire O_2 regime $B > B_{\text{mc}}$.

Finally, at high magnetic fields the layers melt independently following a first-order type 2D melting scenario.

The order parameter μ_0 in the topmost layer then undergoes a finite jump and the surface non-melting (O_1) scenario applies, implying the existence of a second multi-critical point at high fields. Indeed, we do find such a jump at fields of order $10 B_\lambda$, however, a more elaborate version of DFT [18] is required for an accurate determination of this second multi-critical point.

In conclusion, we have analyzed surface melting in the pancake-vortex system of layered superconductors and have found both surface-melting (O_2) and surface-non-melting (O_1) scenarios. The O_2 scenario is realized over most of the low-field phase diagram and explains the experimental observation of asymmetric hysteresis [2].

We acknowledge financial support from the Swiss National Foundation through the program MaNEP and the DST (India).

-
- [1] D.R. Nelson, Phys. Rev. Lett. **60**, 1973 (1988); E. Zeldov *et al.*, Nature **375**, 373 (1995).
 - [2] A. Soibel *et al.*, Nature **406**, 282 (2000).
 - [3] A.R. Ubbelohde, *The Molten State of Matter* (Wiley, New York, 1978); J.W.M. Frenken and J.F. van der Veen, Phys. Rev. Lett. **54**, 134 (1985).
 - [4] U. Tartaglino, T. Zykova-Timan, F. Ercolessi, and E. Tosatti, Physics Reports **411**, 291 (2005).
 - [5] L. Pietronero and E. Tosatti, Solid State Commun. **32**, 255 (1979).
 - [6] R. Lipowsky and W. Speth, Phys. Rev. B **28**, 3983 (1983).
 - [7] A. Trayanov and E. Tosatti, Phys. Rev. Lett. **59**, 2207 (1987).
 - [8] R. Ohnesorge, H. Löwen, and H. Wagner, Phys. Rev. E **50**, 4801 (1994).
 - [9] G. Blatter *et al.*, Rev. Mod. Phys. **66**, 1125 (1994).
 - [10] M.J.W. Dodgson, A.E. Koshelev, V.B. Geshkenbein, and G. Blatter, Phys. Rev. Lett. **84**, 2698 (2000).
 - [11] S. Sengupta *et al.*, Phys. Rev. Lett. **67**, 3444 (1991); G.I. Menon *et al.*, Phys. Rev. B **54**, 16192 (1996); P.S. Cornaglia and C.A. Balseiro, Phys. Rev. B **61**, 784 (2000).
 - [12] H. Fangohr, A.E. Koshelev, and M.J.W. Dodgson, Phys. Rev. B **67**, 174508 (2003).
 - [13] T.V. Ramakrishnan and M. Yussouff, Phys. Rev. B **19**, 2775 (1979); T.V. Ramakrishnan, Phys. Rev. Lett. **48**, 541 (1982).
 - [14] A. De Col *et al.*, *unpublished*.
 - [15] J.P. Hansen and I.R. McDonald, *Theory of Simple Liquids* (Academic Press, London, 1986).
 - [16] We evaluate the first two Fourier coefficients of the relation $\rho_z(\mathbf{R}) = \bar{\rho} \exp[\xi_z(\mathbf{R})]$ and make use of the Ansatz.
 - [17] J.M. Caillol, D. Levesque, J.J. Weis, and J.P. Hansen, J. Stat. Phys. **28**, 325 (1982).
 - [18] Y. Singh, Phys. Rep. **207**, 351 (1991).
 - [19] We drop a small renormalization factor $(1+r)\ell^2\mu''_z \approx \ell^2\mu''_z$ which is absent in the gradient expansion of the bulk equation, the difference being due to our neglecting of higher-order corrections in μ'_z . The factor $(1+r)$ thus is beyond the accuracy of the full non-linear problem.